HOKKAIDO UNIVERSITY

Title	Potential-induced restructuring dynamics of ionic liquids on a gold electrode: Steric effect of constituent ions studied by surface-enhanced infrared absorption spectroscopy
Author(s)	Motobayashi, Kenta; Nishi, Naoya; Inoue, Yuki et al.
Citation	Journal of electroanalytical chemistry, 800, 126-133 https://doi.org/10.1016/j.jelechem.2017.02.049
Issue Date	2017-09-01
Doc URL	https://hdl.handle.net/2115/75313
Rights	© 2017. This manuscript version is made available under the CC-BY-NC-ND 4.0 license http://creativecommons.org/licenses/by-nc-nd/4.0/
Rights(URL)	https://creativecommons.org/licenses/by-nc-nd/4.0/
Type	journal article
File Information	JEAC_Motobayashi.pdf

Hokkaido University Collection of Scholarly and Academic Papers : HUSCAP

Potential-Induced Restructuring Dynamics of Ionic Liquids on a Gold Electrode: Steric Effect of Constituent Ions Studied by Surface-Enhanced Infrared Absorption Spectroscopy

Kenta Motobayashi,[a,b] Naoya Nishi,*[c] Yuki Inoue,[c] Kazuya Minami [c] Tetsuo Sakka,[c] and Masatoshi Osawa[a]*

[a]Institute for Catalysis, Hokkaido University, N21W10, Kita-ku, Sapporo 001-0021, Japan, [b]Department of Physical Science and Engineering, Graduate School of Engineering, Nagoya Institute of Technology, Gokiso-cho, Nagoya, 466-8555, Japan, and [c]Department of Energy and Hydrocarbon Chemistry, Graduate School of Engineering, Kyoto University, Kyoto 615-8510, Japan

AUTHOR INFORMATION

Corresponding Author

kmotobayashi@nitech.ac.jp (K.M.)

nishi.naoya.7e@kyoto-u.ac.jp (N.N.)

ABSTRACT: The structure of the interface between room temperature ionic liquids (RTILs) and an Au electrode changes with applied potential to compensate the charge on the electrode surface. The dynamics of the restructuring of RTILs triggered by the change in potential has been investigated by using surface-enhanced infrared absorption spectroscopy (SEIRAS). To elucidate the effect of steric hindrance of constituent ions on the potential-dependent dynamics, RTILs composed of differently sized ions are examined: imidazolium cations and bis(perfluoroalkylsulfonyl)amide anions with different (perfluoro)alkyl chain length, or tetrafluoroborate anion. The high interface selectivity and sensitivity of SEIRAS enables in-situ, real time observation of dynamic behaviors of both anions and cations during potential scans or steps. During potential scans for RTILs composed of sufficiently large ions (all the RTILs examined in the present study except for that includes BF_4^-), a fast, barrier-less change in local ion concentration occurs in the overlayers first, and then a slow cation-anion replacement occurs in the first ionic layer directly contacting with the electrode surface when an overpotential exceeding a critical value is applied. SEIRAS reveals hysteretic changes of the interfacial structure arising from the ion replacement in the first ionic layer. Potential-dependent SEIRAS measurements for RTILs with different ion sizes highlight the significance of steric hindrance of ions for the ion replacement in the first layer.

HEIGHLIGHT

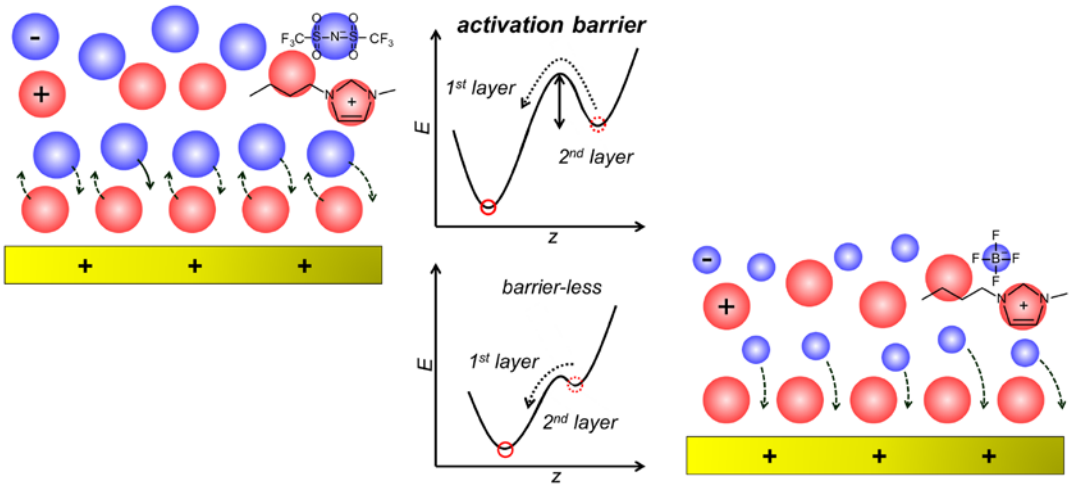
> Dynamics of ionic liquid/Au electrode interfaces were investigated by SEIRAS.

> Differently sized ions were examined to highlight the effect of steric hindrance.

> Hysteretic potential dependence of SEIRAS indicates the barrier for ion replacement.

> Larger ions show higher activation barriers for replacement of the first ionic layer.

GRAPHICAL ABSTRACT



KEYWORDS

spectroelectrochemistry, vibrational spectroscopy, solid/liquid interface, ionic liquid, electrical double layer, surface science

1. Introduction

Room temperature ionic liquids (RTILs), liquid salts at ambient temperature composed purely of cations and anions, have received significant interests as promising electrolyte materials for electrochemical energy devices such as batteries and super capacitors. Their fascinating properties, including high thermal stability, wide electrochemical windows, and high ionic conductivity, are expected to improve the performance and safety of electrochemical devices [1-5]. The RTIL/electrode interface, where electrochemical reactions occur, plays crucial roles in such applications, and hence molecular level description of the interface is necessary for improving the performance of the devices. Gouy-Chapman-Stern (GCS) theory, a conventional model for the electrical double layer at solid/liquid interfaces relying on the dilute-solution approximation, is not directly applicable to RTILs that are full of ionic species [6-8]. Alternatively, multiply-ordered layers of ions or ion pairs have been proposed as a model for the RTIL/electrode interface based upon force curve measurements using atomic force microscope (AFM) [9] and X-ray reflectivity measurements [10], but the details are still under debate [11-13].

The interfacial structure under static conditions has been studied using surface-selective spectroscopies and scanning probe microscopies (SPM). Recent studies with infrared reflection absorption spectroscopy (IRAS) [14, 15], sum frequency generation (SFG) [16-19], surface-enhanced Raman spectroscopy [20, 21], and surface-enhanced infrared absorption spectroscopy (SEIRAS) [22-26] revealed the adsorption of cations on negatively charged electrode surfaces and the replacement of the cations by anions on positively charged surfaces accompanied by a potential-dependent reorientation of the ions. SPM has visualized irreversible morphological

changes of the electrode surface [27, 28] and potential-dependent changes in periodical distribution and mobility of ions over the electrode surface [29-31].

Dynamic behaviors of ions induced by potential changes have also been reported. Cyclic voltammetry (CV), chronoamperometry [32], electrochemical impedance spectroscopy [33], and surface plasmon resonance (SPR) [34] measurements showed very slow relaxation of the electric double layer taking several seconds to tens of minutes. This time scale is much longer than observed at aqueous solution/electrode interfaces (ms to μs time-scale responses [35]). Hysteretic potential-dependence of interfacial restructuring was also observed for some RTILs by electrochemical impedance [33], X-ray reflectometry [36, 37], SFG [18, 19], and SEIRAS [24-26].

Since physical properties of RTILs highly depend on the constituent ions, the structures and dynamics of ions at the electrochemical interface are also expected to depend on the constituent ions. However, no systematic spectroelectrochemical studies have been reported in literature. In the present study, we investigate hysteretic behaviors of ions near the interfaces between various RTILs and a gold electrode to discuss structural effects of constituent ions on the dynamics by using SEIRAS, a powerful vibrational spectroscopic tool to investigate the electrochemical interface. Since the SEIRA effect is significant at the surface and fades away within a few monolayer distance from the surface [38], the background absorption of the bulk RTILs probed by an evanescent wave that penetrates into the bulk solution can completely be eliminated by taking potential difference spectra [39, 40]. The RTILs composed of different combinations of cations and anions depicted in Scheme 1 are used in the present work: 1-butyl-3-methylimidazolium (C_4mim), 1-octyl-3-methylimidazolium (C_8mim), and 1-dodecyl-3-methylimidazolium (C_{12}mim) as the cation, and bis(trifluoromethanesulfonyl)amide (TFSA),

bis(nonafluorobutanesulfonyl)amide (NFSA), and tetrafluoroborate (BF_4) as the anion. From a comparison of [C_4mim][TFSA], [C_8mim][TFSA], and [C_{12}mim][TFSA], the size effect of the neutral alkyl chain of the cation is addressed, whereas the size effect of the anion is addressed by comparing [C_4mim][TFSA], [C_4mim][NFSA], and [C_4mim][BF_4]. We will show that the steric hindrance of ions and ion-ion interactions are decisive factors rather than ion-electrode interaction for hysteretic replacement of the ions in the first layer.

2. Experimental

[C_4mim][TFSA] and [C_4mim][BF_4] (Iolitec, 99 %) were purified by column chromatography [41] and dried in vacuum at 80 °C for overnight to eliminate water and other gaseous contaminants. [C_8mim][TFSA], [C_{12}mim][TFSA], and [C_4mim][NFSA] were synthesized by the method described elsewhere [42, 43] and dried in vacuum as for [C_4mim][TFSA] and [C_4mim][BF_4] just before using.

Potentials of zero total charge (pztc) of a gold wire electrode (Ichimura metals, 99.95 %, diameter of 0.5 mm) in the RTILs were measured by the electrode immersion method [44], in which the charge of the electrode surface, q, was obtained by integrating the current flowed after immersing the Au electrode into the RTILs at a fixed applied potential E. The measurement of the current was repeated for 10 times at each potential E and the averaged q value was plotted against E. The potential at which the q-E plot crosses the zero line, i.e., pztc, was obtained by linear least square fitting. A platinum mesh was used as a counter electrode. An Ag/Ag^+ electrode, a silver wire immersed in RTILs saturated with $AgCF_3SO_3$ and separated from the analyte with a Vycor glass filter, was used as a reference electrode. Potential is quoted with respect to the redox potential of ferrocene (Fc/Fc^+) throughout the paper. Electrode potential was

controlled by a potentiostat (BAS, model 2323). All the measurements were performed in a vacuum chamber (1×10^{-6} Torr).

In SEIRAS measurements, a polycrystalline Au thin film deposited on a nondoped Si hemicylinder prism (Pier Optics) by an electroless deposition technique [45] was used as the working electrode. The Au-coated prism was attached, via a vacuum O-ring (Kalrez®), to a vacuum compatible glass cell equipped with a Pt wire quasi reference electrode and a Pt mesh counter electrode. The Au thin film electrode surface was cleaned by repeating potential cycles in 0.01 M H_2SO_4 aqueous solution until stable voltammograms were obtained, which was followed by rinsing with pure water and drying in a vacuum dryer. After filling up with pre-evacuated RTILs, the spectroelectrochemical cell was evacuated to 5×10^{-6} Torr at 80 °C for overnight before the experiments. The vacuum condition was kept during all measurements. The potential of the Au electrode was controlled by a potentiostat (CHI, 614A) and calibrated by Fc/Fc^+. SEIRA spectra were recorded in the Kretschmann attenuated total reflection (ATR) configuration [38] with a FT-IR spectrometer (DigiLab, FTS-7000) equipped with a HgCdTe (MCT) detector. The spectral resolution used was 4 cm^{-1}.

3. Results and discussion

3.1. [C_4mim][TFSA]

A CV for an Au thin film electrode in [C_4mim][TFSA], Fig. 1(a), shows an electrochemical window of ~4.0 V. The *E*-*q* plot for this system measured by the electrode immersion method is shown in Fig. 1(b). By the linear least square fitting, pztc is determined to be -0.74 V vs Fc/Fc^+. Small cathodic peaks found at $E < -1$ V are possibly due to the surface reconstruction of Au [46] which was reported by electrochemical STM studies of a single crystal surface [27, 28]. Such a

surface reconstruction on a monatomic-scale has negligible effect on SEIRAS which originates from much larger surface roughness in the tens of nanometer-scale.

Figure 2 shows SEIRA spectra of the [C_4mim][TFSA]/Au interface collected during a potential scan from -2.1 to 0.9 V vs Fc/Fc^+ where no Faradaic current was observed (Fig. 1(a)). The spectrum collected at -2.1 V before the potential scan was used as the reference to compute the potential difference spectra. Since the SEIRA effect is significant at the surface and sharply fades away within a few monolayer distance from the surface [38], the observed potential difference spectra are ascribed mostly to the first ionic layer in direct contact with the electrode surface and to the overlayers to some extent [38, 47, 48]. Positive and negative bands indicate the increase and decrease, respectively, in intensities with respect to the reference spectrum recorded at -2.1 V. Each band in the potential difference spectra can find its counterpart in the IR spectrum of the neat [C_4mim][TFSA] measured with the conventional ATR configuration without the Au film (bottom-most spectrum in Fig. 2). The assignments of the bands [49-51] are shown in Fig. 2 and Table 1. The significant blue-shift of the C-F stretch modes $\nu(CF_3)$ in the SEIRA spectra compared to the spectrum of the bulk originates from the large dispersion of the refractive index of [C_4mim][TFSA] in this spectral range [24, 52, 53].

As the potential is made more positive, the absorption bands of the anion (in the spectral range of 1400-1000 cm^{-1}) increase and those of the alkyl chain $\nu(CH)_{alkyl}$ of the cation (3000-2800 cm^{-1}) decrease their intensities. The result appears to indicate the cation-to-anion replacement. However, the intensities of the C-H stretch modes of the imidazolium ring $\nu(CH)_{ring}$ (3200-3000 cm^{-1}) increase. To understand the result, it should be noted that the intensity is a function not only of concentration but also of the orientation of the molecule of interest due to the surface selection rule in SEIRAS (vibrations that yields oscillating dipoles perpendicular to the surface

are selectively observable [54]). The two $\nu(CH)_{ring}$ modes at 3171 and 3105 cm^{-1} yield oscillating dipoles parallel to the ring, whereas the $\nu(CH)_{alkyl}$ modes yield oscillating dipoles perpendicular to the alkyl chain. Therefore, the increase and decrease in the intensities of the $\nu(CH)_{ring}$ and the $\nu(CH)_{alkyl}$, respectively, indicate the reorientation of the imidazolium ring from a flat orientation to a more vertical one.

Integrated band intensities of the vibrational modes of the cation and the anion taken from a series of spectra acquired during two potential cycles starting from -0.5 V to negative direction are plotted against E in Figs. 3(a) and (b). On the positive-going scan starting from -2.1 V, the intensity of the $\nu(CF_3)$ modes of the anion (sum of the symmetric and asymmetric modes), I_{CF}, increases gradually with potential up to 0.3 V and more steeply at more positive potentials. On the reverse negative-going scan, it decreases gradually with potential down to -1.1 V and steeply at more negative potentials to yield a typical hysteresis curve. The intensity of the $\nu(SO_2)$ modes of the anion, I_{SO}, also yields a similar hysteresis curve. On the other hand, the intensity of the $\nu(CH)_{ring}$ modes of the cation, I_{ring}, increases on the positive-going scan up to 0.3 V and decreases at more positive potentials. The initial increase in I_{ring} at $E < 0.3$ V is ascribed to the reorientation of the cation very likely in the first ionic layer, since reorientation of the cation only in the first layer, not in the bulk, can contribute to compensate surface charge (Note that the reorientation of the cation in the first layer changes the distance between the electrode and the charge center of the cation enabling compensation of surface charge, while the reorientation in the overlayers leads to negligible change in the distance). Taking into account the short-range nature of the SEIRA effect, the decrease in I_{ring} in concomitant with the sharp increase in I_{CF} at $E > 0.3$ V is ascribed to the cation-to-anion replacement in the first layer. Similarly, the decrease in I_{ring} at $E < -1.2$ V on the negative-going potential scan is ascribed to the reorientation to more flat

configuration of the cations that comes to the first layer from the overlayers to replace the anions at this potential range. Given that the first layer is full of cation, the gradual increase (decrease) in I_{CF} at -2.0 – 0.3 V on the positive-going scan (at -1.2 – 0.8 V on the negative-going scan) can be ascribed to the increase (decrease) in anion concentration in the overlayers induced by the change in the surface charge.

This interpretation of the spectra is supported by the comparison with the SFG study of [C_4mim][TFSA] on a Pt polycrystalline electrode reported by Zhou et al. [19] Similar hysteretic trends were found in the SFG band intensities for the anion and were interpreted in terms of the cation-anion replacement in the first layer as in the present SEIRAS study. However, a difference is worth to note that the authors did not observe the gradual increase in SFG intensity corresponding to that of I_{CF} observed by SEIRAS. This difference can be ascribed to the higher interface selectivity of SFG: SEIRA effect is significant at the surface and fades away within several monolayer distance [38], while SFG occurs only at the interface where inversion symmetry is most drastically broken. Accordingly, the gradual change in I_{CF} observed only by SEIRAS is due to the change in the local concentration of the anion in the overlayers, and the steep change observed by both SEIRAS and SFG indicates the local concentration change of ions in the first layer.

As shown in Fig. 3(c), the hysteresis becomes more pronounced with lowering the scan rate, implying that the potential-triggered restructuring of the first ionic layer is a rather slow process. This also implies the origin of hysteresis. So far, two types of hysteresis have been reported for potential-dependent behavior of RTIL/electrode interfaces: one is that becomes less significant, and the other is that becomes more significant with decreasing scan rate. The former type of hysteresis originates from non-equilibrium restructuring of the interface simply due to the slow

response of RTILs against the change in potential [34, 55], found in differential capacitance of [BMIM][OTf]/Au [56] and interfacial tension at RTIL/aqueous solution interface [32]. The latter type was attributed to the existence of an energy barrier for restructuring of the interface, observed in SFG spectra [18, 19], differential capacitances [33, 57], and X-ray reflectometry [36, 37] of several RTIL/electrode interfaces. The latter type of hysteresis observed in the present study suggests the requirement of an overpotential for overcoming the activation barrier for the interfacial restructuring.

To study the relaxation dynamics in more detail, the time evolution of I_{CF} for potential steps was measured as shown in Fig. 3(d). By fitting the data with a simple exponential function, the time constant of the relaxation of I_{CF} is calculated to be 310±20 s and 240±30 s for the step from 0.25 to 0.55 V (cation-to-anion exchange in the first layer) and -0.95 V to -1.25 V (anion-to-cation), respectively. These values are of the same order as the time constants of the potential-dependent relaxation of the trioctylmethylammonium bis(nonafluorobutanesulfonyl)amide on Au probed by SPR [34]. On the other hand, for steps from -0.65 to -0.35 V and -0.05 to -0.35 V (ion exchanges in overlayers), immediate changes in I_{CF} can be found. These results demonstrate that the change in the local ion concentration in overlayers is fast and that the ion replacement in the first ionic layer requiring an overpotential to overcome the activation barrier is slow. The fast and slow dynamics here observed correspond to the gradual and steep changes, respectively, in I_{CF} in Fig. 3(a). This slow ion replacement in the first layer causes the indistinctive hysteresis of I_{CF} at faster scan rate (100 mV/s) shown in Fig. 3(c).

The presence of activation barrier for the ion replacement has been suggested in a molecular dynamics simulation [58]. Double-well shaped potential energy surfaces along the direction perpendicular to the electrode surface were calculated for point charges near the RTIL/electrode

interfaces. An activation barrier can be found between two local potential minima corresponding to the first and second ionic layers, even on the neutrally charged electrode surface.

The reason for the unexpected activation barrier for ion replacement in the first layer can be understood in terms of the layered structure model of RTIL/electrode interfaces [9, 10]. Ions in the first layer are stabilized mainly by the coulombic interaction with the charged electrode, and also by the coulombic interaction with ions in overlayers. As the AFM force curve proved [59], the ordering of ionic layers becomes weaker in the overlayers due to the lower influence of the surface charge. The mixing of ions in the overlayers facilitates the ion exchange in the first layer by reducing the vertical ion-ion coulombic interactions. Accordingly the ion replacement in the first layer occurs after the local concentration change in the over layers. One might think that the first layer is more sensitive to applied potential than the overlayers, but this is not the case for [C_4mim][TFSA].

3.2. Size effect of cation

It is natural to consider that the size of constituent ions affects the potential-triggered restructuring dynamics at the interface. For discussing the size effect of cation, RTILs composed of imidazolium cations with different alkyl chain lengths and the common anion, [C_8mim][TFSA] and [C_{12}mim][TFSA], are compared with [C_4mim][TFSA]. Potential difference SEIRA spectra for these RTILs are shown in Figs. 4(a, b) and 5(a,b). Overall spectral features and their potential dependence are very similar to those of [C_4mim][TFSA]/Au in Fig. 2. Assignments of absorption bands can be made straightforward by consulting with those for [C_4mim][TFSA]. The band at 1270 cm^{-1} for [C_{12}mim][TFSA] is of an unidentified impurity. The orientation of the alkyl chains can be derived from potential-dependent SEIRA intensity of $\nu(CH)_{alkyl}$ shown in Figs. 3(b), 4(d) and 5(d), as discussed in Supporting material. In summary,

alkyl chains become generally more perpendicular to the electrode surface at more positive potentials, and longer alkyl chains ($n \geq 12$ in the present study) show more complex potential dependence probably due to their higher flexibility.

The potential-dependence of each band for all [$C_n$mim][TFSA] (n = 4,8,12) (Figs. 3(a), 4(c) and 5(c)) can be interpreted in terms of the reorientation of the cation as well as the cation-anion replacement in the first layer and overlayers, as in the case of [C_4mim][TFSA]. I_{ring} with weaker intensity and less clear hysteresis for [C_8mim][TFSA] and [C_{12}mim][TFSA] than [C_4mim][TFSA] suggests that the longer the alkyl chain is the reorientation of the cation becomes more difficult, and desorption of the cation with flat orientation shows less significant decrease in I_{ring}. The effect of ion size can be clearly found in the shift of the potential of the inflection point where the cation-to-anion replacement in the first layer starts to occur on the negative-going scan: -1.1, -1.2, -1.4 V for [$C_n$mim][TFSA] (n = 4,8,12), respectively. The inflection points for positive-going scans are almost the same (around 0.3 V). Despite the uncertainty in potential due to the possible shift of the redox potential of Fc/Fc^+ in different RTILs [60], the larger separation of the inflection points found in positive- and negative-going scans with longer alkyl chain is evident. This result can be reasonably explained by the larger steric hindrance of ions impeding the ion replacement.

3.3. Size effect of anion

For discussing the effect of the anion size on the dynamic behavior of RTILs, [C_4mim][BF_4] and [C_4mim][NFSA] are compared with [C_4mim][TFSA]. Figs. 6(a) and (b) shows the SEIRA spectra of [C_4mim][NFSA]/Au at various potentials. For the cation, the band assignments are straightforward and potential-dependent reorientation and desorption are suggested as is the case of [C_4mim][TFSA]. Broad absorption band for C-F stretch modes of -CF_3 and -CF_2 group ν(CF)

ranging at 1150-1300 cm^{-1} additionally appears, and its band shape implies potential-dependent isomerization as discussed in Supporting material.

The potential-dependent SEIRA band intensities of [C_4mim][NFSA] are hysteretic as shown in Fig. 6(c). The separations between pztc measured by the immersion method (-0.01 V, indicated by an arrow in Fig. 6) and the inflection potentials for the cation-to-anion and anion-to-cation exchange in the first layer are 1.0 and 1.2 V, respectively. These values are both larger than corresponding values for [C_4mim][TFSA] (0.4 and 1.0 V, respectively) which shares identical cation with [C_4mim][NFSA]. It means that the larger anion leads to higher activation energy for the exchange of ions in the first layer. In addition, changes in the potential separation for both cation-to-anion and anion-to-cation exchange imply that the activation barrier for the ion replacement is determined not only by the energy required for breaking ion-electrode interactions, but also by ion-ion interactions.

Figures 7(a) and (b) show the SEIRA spectra of [C_4mim][BF_4]/Au at various potentials together with the ATR spectra of the bulk (bottom-most spectra). The band assignment shown in the figures was made in analogy with [C_4mim][TFSA] [50]. The C-N stretch mode of the cation at 1160 cm^{-1} shows a potential dependence similar to $\nu(CH)_{ring}$, both of which yield transition dipoles parallel to the ring plane. A broad absorption band of B-F stretch mode $\nu(BF_4)$, which was obscured by the strong absorption by the Si prism in the earlier SEIRAS study of [C_2mim][BF_4]/Au by Nanbu et al. [22], is clearly resolved and found to increase its intensity as the potential is made more positive, suggesting the approach of the anion to the electrode surface. The blue-shift of $\nu(BF_4)$ in SEIRA spectra compared to the ATR-IR spectrum of the bulk can be explained by the large dispersion of the refractive index [24, 52, 53] or the anion-electrode interaction.

As shown in Fig. 7(c), the potential dependent hysteretic behavior as was observed for the other RTILs is absent for all the vibrational modes, and both I_{ring} and I_{BF} (intensity of $\nu(BF_4)$) continue to increase with potential in the whole potential range examined. I_{ring} increases with potential due to the reorientation, but its decrease at high potentials as observed for [C_4mim][TFSA] originating from the cation-to-anion replacement is not found, implying that anions co-adsorb with cations without desorption of cations. Co-adsorption of a cation with a small anion has also been suggested in SFG studies of [BMIM][$N(CN)_2$] [61] and other RTILs [62] on Pt surfaces. The absence of hysteretic behavior for [C_4mim][BF_4] is ascribed to the easy penetration of small anions into the first cation layer without ion replacement.

The co-adsorption instead of replacement also affects the dynamics of ions as shown in Fig. 7(d), the time evolutions of I_{BF} for potential steps. I_{BF} changes immediately after the potential steps, in marked contrast to I_{CF} for the [C_4mim][TFSA] case taking several minutes. This tendency is opposite to that of viscosity (100 mPa s for [C_4mim][BF_4] and 50 mPa s for [C_4mim][TFSA]), demonstrating that the dynamics of the ion near the interface is not directly related to bulk properties but nano-scale environment near the interface [63].

The quasi-periodic layered interfacial structure of RTILs is stabilized not only by ion-electrode but also by ion-ion coulombic interactions to form Madelung-like potential as discussed in section 3.1. This stabilization is the most conceivable origin of the activation barrier for the ion replacement. In addition to such coulombic interactions, the present results suggest that the steric hindrance of constituent ions of RTILs also contributes to the activation barrier, which acts as “resistance” against the ion replacement. All the above results indicate that the layered structure of the interface is mainly stabilized by ion-electrode and ion-ion coulombic interactions and secondarily supported by the steric hindrance of ions.

4. Conclusions

SEIRAS that selectively probes metal/solution interfaces was used to study the potential-triggered restructuring dynamics of various imidazolium-based RTILs in the vicinity of the Au electrode surface. Potential-dependent reorientation of cations and a hysteretic anion/cation replacement were observed for the most RTILs examined except for that includes BF_4^-. Together with a comparison of an earlier SFG study, the results were interpreted in terms of the generally accepted multi-layered structure of ions. It is revealed that the local ion concentration in the overlayers changes first, and then the hysteretic anion/cation replacement in the first layer occurs to compensate the changes in surface charge, during potential scans. The latter ion replacement in the first layer is slow dynamics taking several minutes due to the presence of an energy barrier of the ion exchange. Larger-sized ions have higher activation barriers for the ion replacement in the first layer. For RTILs constitute of a sufficiently small anion such as BF_4^-, it is likely that the anion can penetrate into the space between cations instead of the anion/cation replacement, and hence do not show hysteretic behaviors. We believe that ion-electrode and ion-ion coulombic interactions stabilize the multi-layered structure of ions near the electrode, and the structural restriction is higher for the first layer, which leads to the activation barrier and the hysteretic behavior. Steric hindrance of ions additionally contributes to the structural restriction of the first layer. The tendency of the hysteretic interfacial restructuring dynamics of RTILs found in the present study helps designing RTIL/electrode interfaces, which is advantageous for improving electrochemical reactions that are sensitive to nano-scale environment near the electrodes.

Acknowledgment

This work was supported by JSPS KAKENHI Grant Number 24550143 and 25810044, the Kurata Research Grant, and the Cooperative Research Program of Catalysis Research Center

from Hokkaido University (No. 12A0003, 13A1006 and 14B1010). The authors thank the technical division of Institute for Catalysis, Hokkaido University for their help in manufacturing the experimental equipment.

References

[1] M.C. Buzzeo, R.G. Evans, R.G. Compton, Non-Haloaluminate Room-Temperature Ionic Liquids in Electrochemistry—A Review, ChemPhysChem 5 (2004) 1106-20.

[2] M. Galiński, A. Lewandowski, I. Stępniak, Ionic liquids as electrolytes, Electrochim. Acta 51 (2006) 5567-80.

[3] P. Hapiot, C. Lagrost, Electrochemical Reactivity in Room-Temperature Ionic Liquids, Chem. Rev. 108 (2008) 2238-64.

[4] H. Ohno, Electrochemical aspects of ionic liquids, Wiley, Hoboken, 2011.

[5] A. A. J. Torriero, M.J.A. Ahiddiky, Electrochemical properties and applications of ionic liquids, Nova, New York, 2011.

[6] A.A. Kornyshev, Double-Layer in Ionic Liquids: Paradigm Change?, J. Phys. Chem. B 111 (2007) 5545-57.

[7] M.V. Fedorov, A.A. Kornyshev, Ionic Liquid Near a Charged Wall: Structure and Capacitance of Electrical Double Layer, J. Phys. Chem. B 112 (2008) 11868-72.

[8] K.B. Oldham, A Gouy-Chapman-Stern model of the double layer at a (metal)/(ionic liquid) interface, J. Electroanal. Chem. 613 (2008) 131-8.

[9] R. Hayes, G.G. Warr, R. Atkin, At the interface: solvation and designing ionic liquids, Phys. Chem. Chem. Phys. 12 (2011) 1709-23.

[10] M. Mezger, H. Schröder, H. Reichert, S. Schramm, J.S. Okasinski, S. Schöder, V. Honkimäki, M. Deutsch, B.M. Ocko, J. Ralston, M. Rohwerder, M. Stratmann, H. Dosch, Molecular Layering of Fluorinated Ionic Liquids at a Charged Sapphire (0001) Surface, Science 322 (2008) 424-8.

[11] M.V. Fedorov, A.A. Kornyshev, Ionic Liquids at Electrified Interfaces, Chem. Rev. 114 (2014) 2978-3036.

[12] A.A. Kornyshev, R. Qiao, Three-Dimensional Double Layers, J. Phys. Chem. C 118 (2014) 18285-90.

[13] R. Hayes, G.G. Warr, R. Atkin, Structure and Nanostructure in Ionic Liquids, Chem. Rev. 115 (2015) 6357-426.

[14] N. Nanbu, Y. Sasaki, F. Kitamura, In situ FT-IR spectroscopic observation of a room-temperature molten salt gold electrode interphase, Electrochem. Commun. 5 (2003) 383-7.

[15] O. Höfft, S. Bahr, V. Kempter, Investigations with Infrared Spectroscopy on Films of the Ionic Liquid [EMIM]Tf_2N, Langmuir 24 (2008) 11562-6.

[16] S. Baldelli, Surface Structure at the Ionic Liquid-Electrified Metal Interface, Acc. Chem. Res. 41 (2008) 421-31.

[17] B. Bozzini, A. Bund, B. Busson, C. Humbert, A. Ispas, C. Mele, A. Tadjeddine, An SFG/DFG investigation of CN^- adsorption at an Au electrode in 1-butyl-1-methyl-pyrrolidinium bis(trifluoromethylsulfonyl) amide ionic liquid, Electrochem. Commun. 12 (2010) 56-60.

[18] W. Zhou, S. Inoue, T. Iwahashi, K. Kanai, K. Seki, T. Miyamae, D. Kim, Y. Katayama, Y. Ouchi, Double layer structure and adsorption/desorption hysteresis of neat ionic liquid on Pt electrode surface - an in-situ IR-visible sum-frequency generation spectroscopic study, Electrochem. Commun. 12 (2010) 672-5.

[19] W. Zhou, Y. Xu, Y. Ouchi, Hysteresis Effects in the In Situ SFG and Differential Capacitance Measurements on Metal Electrode/Ionic Liquids Interface, ECS Transactions 50 (2013) 339-48.

[20] V.O. Santos, M.B. Alves, M.S. Carvalho, P.A.Z. Suarez, J.C. Rubim, Surface-Enhanced Raman Scattering at the Silver Electrode/Ionic Liquid ($BMIPF_6$) Interface, J. Phys. Chem. B 110 (2006) 20379-85.

[21] Y.-X. Yuan, T.-C. Niu, M.-M. Xu, J.-L. Yao, R.-A. Gu, Probing the adsorption of methylimidazole at ionic liquids/Cu electrode interface by surface-enhanced Raman scattering spectroscopy, J. Raman Spectrosc. 41 (2009) 516-23.

[22] N. Nanbu, T. Kato, Y. Sasaki, F. Kitamura, In Situ SEIRAS Study of Room-temperature Ionic Liquid | Gold Electrode Interphase, Electrochemistry 73 (2005) 610-3.

[23] Y.-Y. Yang, L.-N. Zhang, M. Osawa, W.-B. Cai, Surface-Enhanced Infrared Spectroscopic Study of a CO-Covered Pt Electrode in Room-Temperature Ionic Liquid, J. Phys. Chem. Lett. 4 (2013) 1582-6.

[24] K. Motobayashi, K. Minami, N. Nishi, T. Sakka, M. Osawa, Hysteresis of Potential-Dependent Changes in Ion Density and Structure of an Ionic Liquid on a Gold Electrode: In Situ Observation by Surface-Enhanced Infrared Absorption Spectroscopy, J. Phys. Chem. Lett. 4 (2013) 3110-4.

[25] K. Motobayashi, M. Osawa, Potential-dependent condensation of Water at the Interface between ionic liquid [BMIM][TFSA] and an Au electrode, Electrochem. Commun. 65 (2016) 14-7.

[26] N. Nishi, K. Minami, K. Motobayashi, M. Osawa, T. Sakka, Interfacial Structure at the Quaternary Ammonium-Based Ionic Liquids|Gold Electrode Interface Probed by Surface-Enhanced Infrared Absorption Spectroscopy: Anion Dependence of the Cationic Behavior, J. Phys. Chem. C 121 (2017) 1658-66.

[27] L.G. Lin, Y. Wang, J.W. Yan, Y.Z. Yuan, J. Xiang, B.W. Mao, An in situ STM study on the long-range surface restructuring of Au(111) in a non-chloroaluminumated ionic liquid, Electrochem. Commun. 5 (2003) 995-9.

[28] N. Borisenko, S. Zein El Abedin, F. Endres, In Situ STM Investigation of Gold Reconstruction and of Silicon Electrodeposition on Au(111) in the Room Temperature Ionic Liquid 1-Butyl-1-methylpyrrolidinium Bis(trifluoromethylsulfonyl)imide, J. Phys. Chem. B 110 (2006) 6250-6.

[29] Y.-Z. Su, Y.-C. Fu, J.-W. Yan, Z.-B. Chen, B.-W. Mao, Double Layer of Au(100)/Ionic Liquid Interface and Its Stability in Imidazolium-Based Ionic Liquids, Angew. Chem. Int. Ed. 48 (2009) 5148-51.

[30] R. Wen, B. Rahn, O.M. Magnussen, Potential-Dependent Adlayer Structure and Dynamics at the Ionic Liquid/Au(111) Interface: A Molecular-Scale In Situ Video-STM Study, Angew. Chem. Int. Ed. 54 (2015) 6062-6.

[31] A. Elbourne, S. McDonald, K. Voïchovsky, F. Endres, G.G. Warr, R. Atkin, Nanostructure of the Ionic Liquid–Graphite Stern Layer, ACS Nano 9 (2015) 7608-20.

[32] Y. Yasui, Y. Kitazumi, R. Ishimatsu, N. Nishi, T. Kakiuchi, Ultraslow Response of Interfacial Tension to the Change in the Phase-Boundary Potential at the Interface between Water and a Room-Temperature Ionic Liquid, Trioctylmethylammonium bis(nonafluorobutanesulfonyl)amide, J. Phys. Chem. B 113 (2009) 3273-6.

[33] M. Drüschler, B. Huber, S. Passerini, B. Roling, Hysteresis Effects in the Potential-Dependent Double Layer Capacitance of Room Temperature Ionic Liquids at a Polycrystalline Platinum Interface, J. Phys. Chem. C 114 (2010) 3614-7.

[34] N. Nishi, Y. Hirano, T. Motokawa, T. Kakiuchi, Ultraslow relaxation of the structure at the ionic liquid|gold electrode interface to a potential step probed by electrochemical surface plasmon resonance measurements: asymmetry of the relaxation time to the potential-step direction, Phys. Chem. Chem. Phys. 15 (2013) 11615-9.

[35] A. Yamakata, M. Osawa, Dynamics of Double-Layer Restructuring on a Platinum Electrode covered by CO: Laser-Induced Potential Transient Measurement, J. Phys. Chem. C 112 (2008) 11427-32.

[36] A. Uysal, H. Zhou, G. Feng, S.S. Lee, S. Li, P. Fenter, P.T. Cummings, P.F. Fulvio, S. Dai, J.K. McDonough, Y. Gogotsi, Structural Origins of Potential Dependent Hysteresis at the Electrified Graphene/Ionic Liquid Interface, J. Phys. Chem. C 118 (2014) 569-74.

[37] A. Uysal, H. Zhou, G. Feng, S.S. Lee, S. Li, P.T. Cummings, P.F. Fulvio, S. Dai, J.K. McDonough, Y. Gogotsi, P. Fenter, Interfacial ionic 'liquids': connecting static and dynamic structures, J. Phys.: Condens. Matter 27 (2015) 032101.

[38] M. Osawa, Dynamic Processes in Electrochemical Reactions Studied by Surface-Enhanced Infrared Absorption Spectroscopy (SEIRAS), Bull. Chem. Soc. Jpn. 70 (1997) 2861-80.

[39] K. Ataka, T. Yotsuyanagi, M. Osawa, Potential-Dependent Reorientation of Water Molecules at an Electrode/Electrolyte Interface Studied by Surface-Enhanced Infrared Absorption Spectroscopy, J. Phys. Chem. 100 (1996) 10664-72.

[40] M. Osawa, M. Tsushima, H. Mogami, G. Samjeske, A. Yamakata, Structure of Water at the Electrified Platinum-Water Interface: A Study by Surface-Enhanced Infrared Absorption Spectroscopy, J. Phys. Chem. C 112 (2008) 4248-56.

[41] M.J. Earle, C.M. Gordon, N.V. Plechkova, K.R. Seddon, T. Welton, Decolorization of Ionic Liquids for Spectroscopy, Anal. Chem. 79 (2006) 758-64.

[42] T. Kakiuchi, N. Tsujioka, S. Kurita, Y. Iwami, Phase-boundary potential across the nonpolarized interface between the room-temperature molten salt and water, Electrochem. Commun. 5 (2003) 159-64.

[43] N. Nishi, H. Murakami, Y. Yasui, T. Kakiuchi, Use of Highly Hydrophobic Ionic Liquids for Ion-selective Electrodes of the Liquid Membrane Type, Anal. Sci. 24 (2008) 1315-20.

[44] V. Jendrasic, Immersion-electrode method for the determination of the point of zero charge of solid metals, Journal of Electroanalytical Chemistry and Interfacial Electrochemistry 22 (1969) 157-64.

[45] H. Miyake, S. Ye, M. Osawa, Electroless deposition of gold thin films on silicon for surface-enhanced infrared spectroelectrochemistry, Electrochem. Commun. 4 (2002) 973-7.

[46] A.A. Kornyshev, I. Vilfan, Phase transitions at the electrochemical interface, Electrochim. Acta 40 (1995) 109-27.

[47] E. Johnson, R. Aroca, Surface-enhanced infrared spectroscopy of monolayers, J. Phys. Chem. 99 (1995) 9325-30.

[48] T. Kamata, A. Kato, J. Umemura, T. Takenaka, Intensity enhancement of infrared attenuated total reflection spectra of stearic acid Langmuir-Blodgett monolayers with evaporated silver island films, Langmuir 3 (1987) 1150-4.

[49] M. Herstedt, M. Smirnov, P. Johansson, M. Chami, J. Grondin, L. Servant, J.C. Lassègues, Spectroscopic characterization of the conformational states of the bis(trifluoromethanesulfonyl)imide anion ($TFSI^-$), J. Raman Spectrosc. 36 (2005) 762-70.

[50] S.A. Katsyuba, E.E. Zvereva, A. Vidiš, P.J. Dyson, Application of Density Functional Theory and Vibrational Spectroscopy Toward the Rational Design of Ionic Liquids, J. Phys. Chem. A 111 (2007) 352-70.

[51] I. Rey, P. Johansson, J. Lindgren, J.C. Lassègues, J. Grondin, L. Servant, Spectroscopic and Theoretical Study of $(CF_3SO_2)_2N^-$ ($TFSI^-$) and $(CF_3SO_2)_2NH$ (HTFSI), J. Phys. Chem. A 102 (1998) 3249-58.

[52] J. Pacansky, C.D. England, R. Waltman, Infrared Spectroscopic Studies of Poly(perfluoropropyleneoxide) on Gold Substrates: A Classical Dispersion Analysis for the Refractive Index, Appl. Spectrosc. 40 (1986) 8-16.

[53] T. Buffeteau, J. Grondin, J.-C. Lassègues, Infrared Spectroscopy of Ionic Liquids: Quantitative Aspects and Determination of Optical Constants, Appl. Spectrosc. 64 (2010) 112-9.

[54] M. Osawa, K. Ataka, K. Yoshii, Y. Nishikawa, Surface-Enhanced Infrared Spectroscopy: The Origin of the Absorption Enhancement and Band Selection Rule in the Infrared Spectra of Molecules Adsorbed on Fine Metal Particles, Appl. Spectrosc. 47 (1993) 1497-502.

[55] S. Makino, Y. Kitazumi, N. Nishi, T. Kakiuchi, Charging current probing of the slow relaxation of the ionic liquid double layer at the Pt electrode, Electrochem. Commun. 13 (2011) 1365-8.

[56] T.R. Gore, T. Bond, W. Zhang, R.W.J. Scott, I.J. Burgess, Hysteresis in the measurement of double-layer capacitance at the gold-ionic liquid interface, Electrochem. Commun. 12 (2010) 1340-3.

[57] M. Drüschler, B. Huber, B. Roling, On Capacitive Processes at the Interface between 1-Ethyl-3-methylimidazolium tris(pentafluoroethyl)trifluorophosphate and Au(111), J. Phys. Chem. C 115 (2011) 6802-8.

[58] V. Ivaništšev, M.V. Fedorov, R.M. Lynden-Bell, Screening of Ion–Graphene Electrode Interactions by Ionic Liquids: The Effects of Liquid Structure, J. Phys. Chem. C 118 (2014) 5841-7.

[59] R. Hayes, N. Borisenko, M.K. Tam, P.C. Howlett, F. Endres, R. Atkin, Double Layer Structure of Ionic Liquids at the Au(111) Electrode Interface: An Atomic Force Microscopy Investigation, J. Phys. Chem. C 115 (2011) 6855-63.

[60] A.A.J. Torriero, P.C. Howlett, Ionic liquid effects on the redox potential of ferrocene, Electrochem. Commun. 16 (2012) 84-7.

[61] C. Aliaga, S. Baldelli, Sum Frequency Generation Spectroscopy and Double-Layer Capacitance Studies of the 1-Butyl-3-Methylimidazolium Dicyanamide/Platinum Interface, J. Phys. Chem. B 110 (2006) 18481-91.

[62] S. Baldelli, Interfacial Structure of Room-Temperature Ionic Liquids at the Solid–Liquid Interface as Probed by Sum Frequency Generation Spectroscopy, J. Phys. Chem. Lett. 4 (2012) 244-52.

[63] Y. Yasui, Y. Kitazumi, H. Mizunuma, N. Nishi, T. Kakiuchi, A comparison of the ultraslow relaxation processes at the ionic liquid|water interface for three hydrophobic ionic liquids, Electrochem. Commun. 12 (2010) 1479-82.

Figure captions

Scheme 1. The chemical structures of ions constituting the RTILs utilized in the present study. (a) $C_n mim^+$ (n = 4,8,12), (b) $TFSA^-$, (c) BF_4^-, (d) $NFSA^-$. The index of carbon atom is also shown in (a).

Fig. 1. (a) CV of [C_4mim][TFSA]/Au at scan rate of 100 mV/s [24]. (b) The surface charge of Au electrodes as a function of the potential in [C_4mim][TFSA] measured by electrode immersion method in vacuum condition (1×10^{-6} Torr). The red line is the result of least square fitting of the data points, indicating that pztc, the potential at which q = 0, is -0.74 V.

Fig. 2. SEIRA spectra of [C_4mim][TFSA]/Au at (a) 3200-2800 cm^{-1} and (b) 1400-1000 cm^{-1} recorded at various electrode potentials during the positive-going scan at 2 mV/s. The reference spectrum was collected at -2.1 V vs Fc/Fc^+. The bottom-most spectra are ATR-IR spectra of [C_4mim][TFSA] reflecting the bulk vibrational features.

Fig. 3. (a), (b) SEIRA band intensities of [C_4mim][TFSA]/Au as a function of electrode potential recorded during the potential scans at 2 mV/s. Band intensities are obtained by direct integration of SEIRA spectra with respect to a local baseline. I_{ring}, I_{SO}, I_{CF}, $I_{(CH2)s}$, $I_{(CH3)s}$, $I_{(CH2)as}$, and $I_{(CH3)as}$ are the total intensities of the bands at 3171, 3120, and 3105 cm^{-1}; 1357 and 1327 cm^{-1}; 1238 and 1221 cm^{-1}; 2863 cm^{-1}; 2874 cm^{-1}; 2934 cm^{-1}; and 2959 cm^{-1}, respectively. The results for two cycles of potential scans, which start and end at -0.3 V, are shown. Pztc is depicted as arrows. I_{CF} as a function of the potential at the scan rate of 2 (circles), 25 (triangles), and 500 mV/s (crosses). (d) I_{CF} as a function of time recorded before and after a potential step at 400 s. The parameters of the potential steps are indicated in the figure.

Fig. 4. (a), (b) SEIRA spectra of [C_8mim][TFSA]/Au recorded at various electrode potentials during the positive-going scan at 2 mV/s. The reference spectrum was collected at -2.4 V vs

Fc/Fc^+. The bottom-most spectra are ATR-IR spectra of $[C_8mim][TFSA]$. (c), (d) SEIRA band intensities as a function of electrode potential recorded during the potential scans at 2 mV/s. The results for two cycles of potential scans, which start and end at -0.9 V, are shown. I_{ring}, I_{SO}, I_{CF}, $I_{(CH2)s}$, $I_{(CH3)s}$, $I_{(CH2)as}$, and $I_{(CH3)as}$ are the total intensities of the bands at 3169, 3119, and 3106 cm^{-1}; 1355 and 1327 cm^{-1}; 1236 and 1210 cm^{-1}; 2851 cm^{-1}; 2872 cm^{-1}; 2922 cm^{-1}; and 2957 cm^{-1}, respectively.

Fig. 5. (a), (b) SEIRA spectra of $[C_{12}mim][TFSA]$/Au recorded at various electrode potentials during the positive-going scan at 2 mV/s. The reference spectrum was collected at -2.4 V vs Fc/Fc^+. The bottom-most spectra are ATR-IR spectra of $[C_{12}mim][TFSA]$. (c), (d) SEIRA band intensities as a function of electrode potential recorded during the potential scans at 2 mV/s. The results for two cycles of potential scans, which start and end at -0.9 V, are shown. I_{ring}, I_{SO}, I_{CF}, $I_{(CH2)s}$, $I_{(CH3)s}$, $I_{(CH2)as}$, and $I_{(CH3)as}$ are the total intensities of the bands at 3163, 3119, and 3099 cm^{-1}; 1354 and 1327 cm^{-1}; 1228 and 1208 cm^{-1}; 2851 cm^{-1}; 2875 cm^{-1}; 2924 cm^{-1}; and 2960 cm^{-1}, respectively.

Fig. 6. (a), (b) SEIRA spectra of $[C_4mim][NFSA]$/Au recorded at various electrode potentials during the positive-going scan at 2 mV/s. The reference spectrum was collected at -2.3 V vs Fc/Fc^+. The bottom-most spectra are ATR-IR spectra of $[C_4mim][NFSA]$. (c), (d) SEIRA band intensities as a function of electrode potential recorded during a potential scan at 2 mV/s which start and end at -0.3 V. I_{ring}, I_{SO}, I_{CF}, $I_{(CH2)s}$, $I_{(CH3)s}$, $I_{(CH2)as}$, and $I_{(CH3)as}$ are the total intensities of the bands at 3167, 3126, and 3103 cm^{-1}; 1354 and 1328 cm^{-1}; 1259, 1229, 1209 and 1187 cm^{-1}; 2860 cm^{-1}; 2876 cm^{-1}; 2935 cm^{-1}; and 2963 cm^{-1}, respectively.

Fig. 7. (a), (b) SEIRA spectra of $[C_4mim][BF_4]$/Au recorded at various electrode potentials during the positive-going scan at 25 mV/s. The reference spectrum was collected at -2.7 V vs

Fc/Fc^+. The bottom-most spectra are ATR-IR spectra of [C_4mim][BF_4]. (c) SEIRA band intensities as a function of electrode potential recorded during the potential scans at 2 mV/s. The results for two cycles of potential scans, which start and end at -0.9 V, are shown. I_{ring}, I_{alkyl}, I_{CN}, and I_{BF} are the total intensities of the bands at 3171, 3123, and 3110 cm^{-1}; 2862 cm^{-1}, 2873 cm^{-1}, 2931 cm^{-1} and 2960 cm^{-1}; 1170 cm^{-1}; and 1087 cm^{-1}, respectively. (d) I_{BF} and I_{alkyl} as a function of time recorded before and after potential step at 400 s.

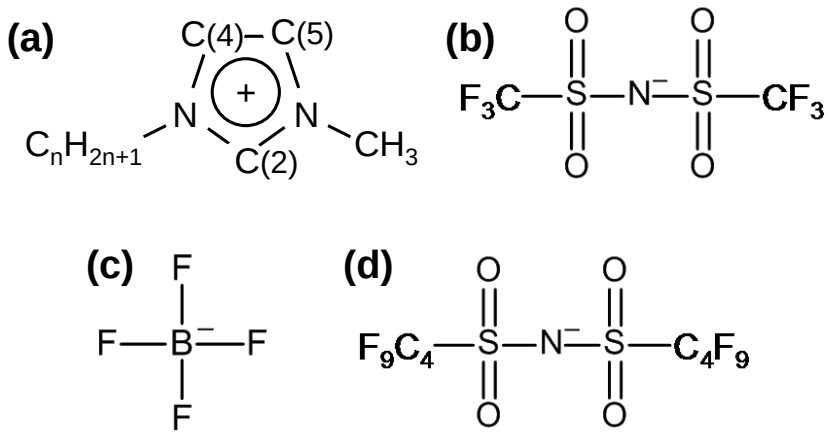
Table 1. Vibrational frequencies (cm^{-1}) and assignments of [C_4mim][TFSA].

SEIRAS	ATR-IR	Calculation	Assignment
3171	3157	3178[a]	ν(C(4)-H, C(5)-H)$_{ring}$ out-of-phase
3120	3123	3122[a]	ν(C(2)-H)$_{ring}$
3105	3105		
2959	2969	2957[a]	$\nu_{as}(CH_3)_{alkyl}$
2934	2941	2939[a]	$\nu_{as}(CH_2)_{alkyl}$
2874	2882	2871[a]	$\nu_{s}(CH_3)_{alkyl}$
2863	2870	2857[a]	$\nu_{s}(CH_2)_{alkyl}$
1357	1355	1323[b]	$\nu_{as}(SO_2)$
1327	1332	1300[b]	$\nu_{as}(SO_2)$
1238	1203	1234[b]	$\nu_{s}(CF_3)$
1221	1191	1205[b]	$\nu_{as}(CF_3)$
1134	1140	1112[b]	$\nu_{s}(SO_2)$
1060	1059	999[b]	ν_{as}(SNS)

ν: stretching, s: symmetric; as: asymmetric; and C(2), C(4) and C(5): indicated in Scheme 1.

a: Reference [50].

b: Reference [49].



Scheme 1

Motobayashi et al.

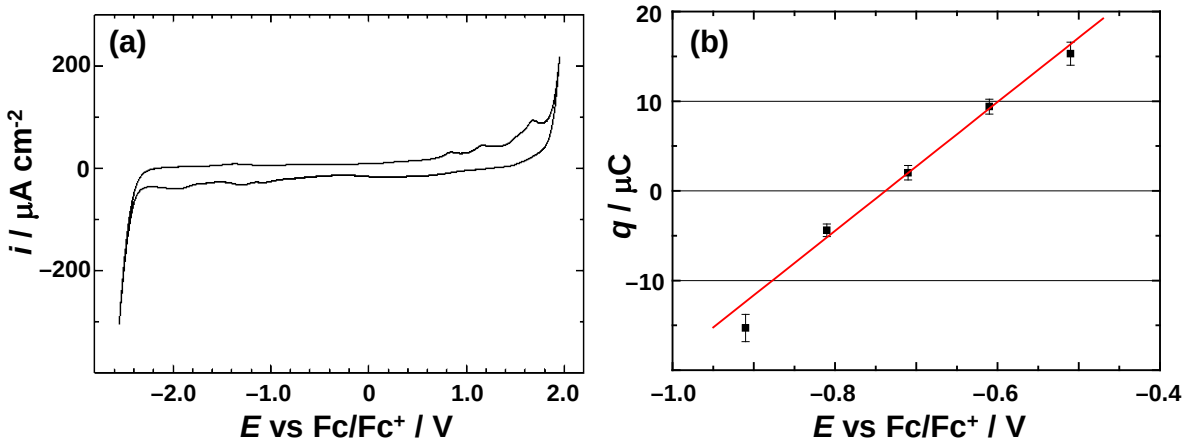


Figure 1

Motobayashi et al.

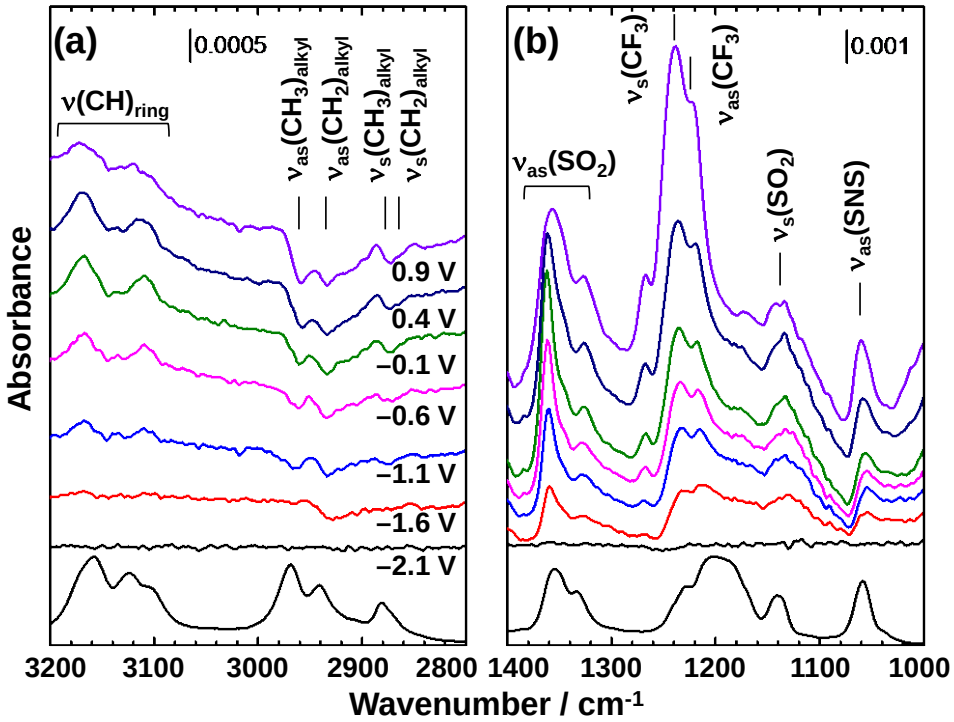


Figure 2

Motobayashi et al.

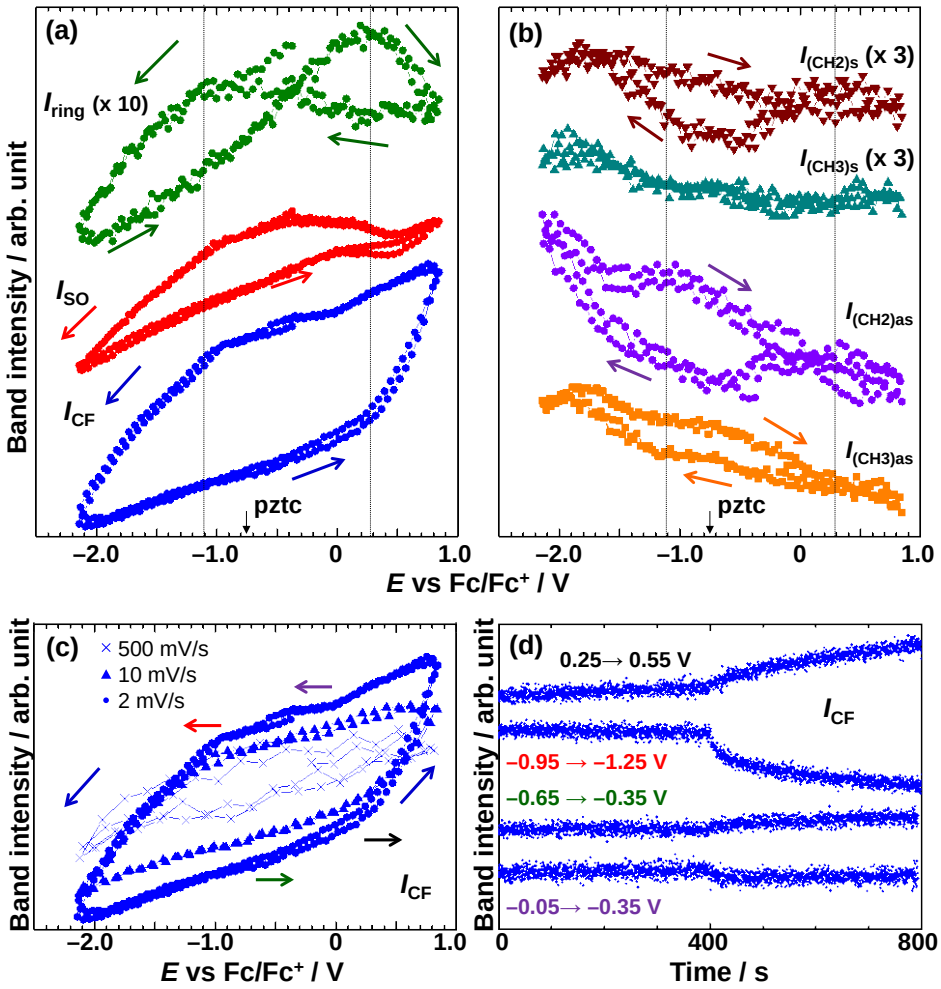


Figure 3

Motobayashi et al.

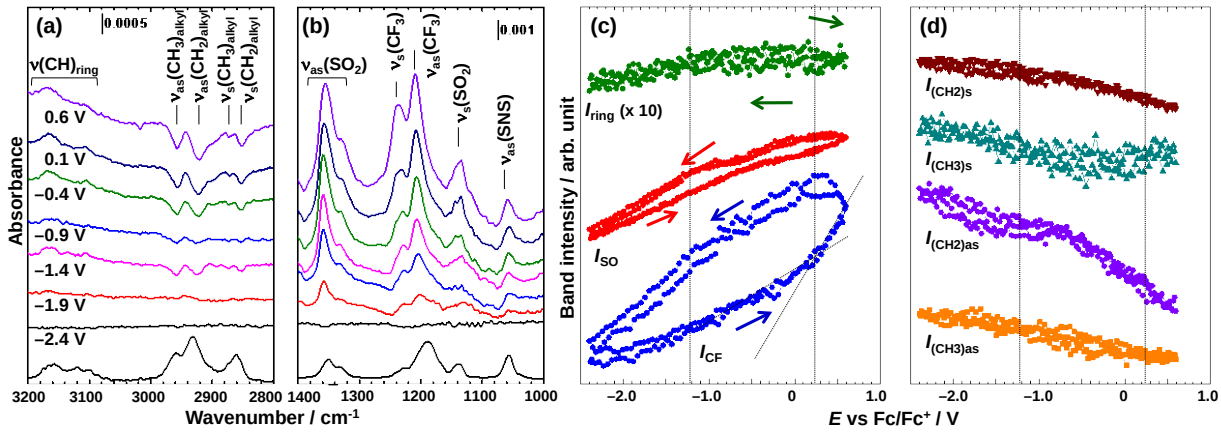


Figure 4

Motobayashi et al.

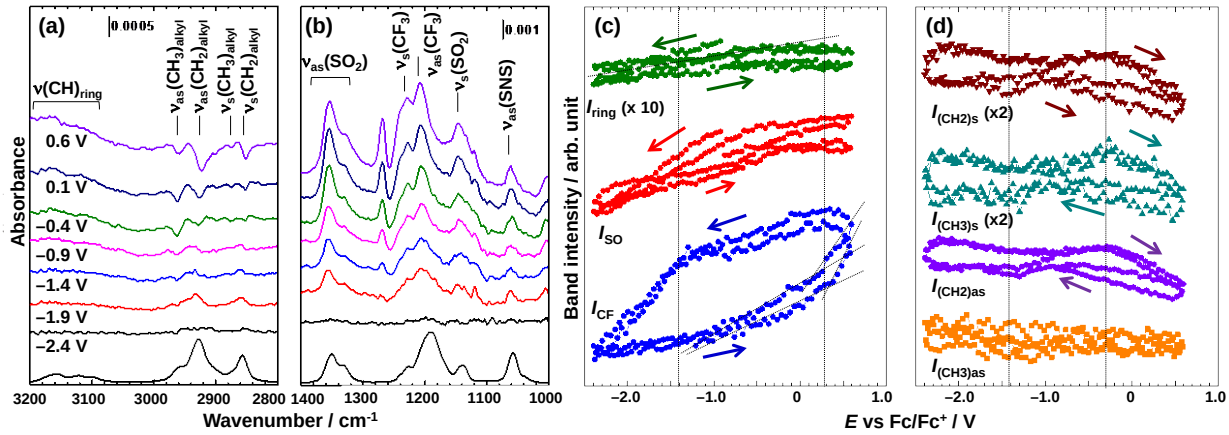


Figure 5

Motobayashi et al.

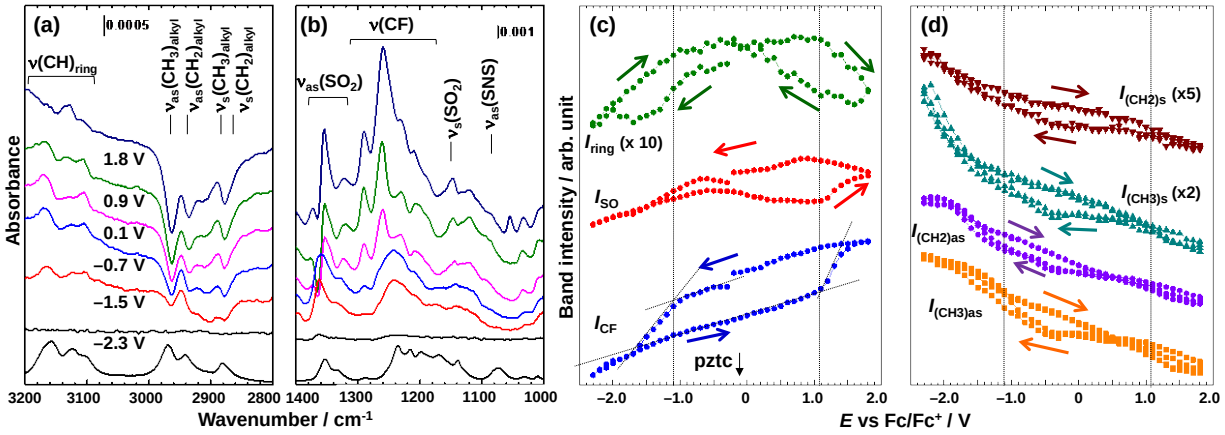


Figure 6

Motobayashi et al.

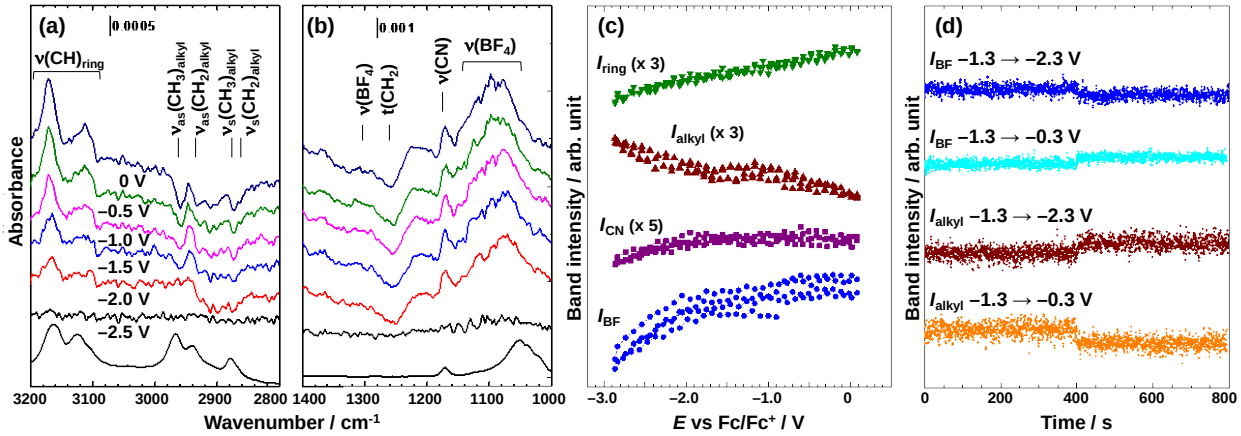


Figure 7

Motobayashi et al.